A survey of xenon ion sputter yield data and fits relevant to electric propulsion spacecraft integration

IEPC-2017-060

John T. Yim[1]
NASA Glenn Research Center, Cleveland, OH, 44135, USA

A survey of low energy xenon ion impact sputter yields was conducted to provide a more coherent baseline set of sputter yield data and accompanying fits for electric propulsion integration. Data uncertainties are discussed and different available curve fit formulas are assessed for their general suitability. A Bayesian parameter fitting approach is used with a Markov chain Monte Carlo method to provide estimates for the fitting parameters while characterizing the uncertainties for the resulting yield curves.

Nomenclature

E	= Ion energy [eV]		e	= Elementary charge = $1.602{\times}10^{-19}$ C
M	= Atomic weight [g/mol]		j	= Current density [A/m^2]
P	= Pressure [Pa]		k	= Boltzmann constant = $1.38{\times}10^{-23}$ J/K
R	= Normalized residual [-]		m	= Particle mass [kg]
R_0	= Average lattice constant [Å]		n	= Number density [1/m^3]
S_n	= Nuclear stopping cross section [eV Å^2]		s_n	= Reduced nuclear stopping power [-]
T	= Temperature [K]		ϵ	= Reduced energy [-]
U_s	= Surface binding energy [eV]		ε_0	= Vacuum permittivity = $8.854{\times}10^{-12}$ F/m
Y	= Sputter yield [atom/ion *or* mm^3/C]			= $1.42{\times}10^{-40}$ C^2/eV/Å
Y'	= Normalized angular sputter yield [-]		θ	= Ion incident angle [deg]
Z	= Atomic number [-]			
a_0	= Bohr radius = 0.529 Å		Subscripts:	
a_{BM}	= Sigmund Born-Mayer potential		i	= Projectile ion
	screening length = 0.219 Å		s	= Target surface material
a_L	= Lindhard screening length [Å]			

I.   Introduction

AS electric propulsion (EP) technology continues to increase its use and expand its operational envelopes through growth in throughput and power,[1] proper assessment of spacecraft integration becomes key to its success. One area of concern for long duration EP operation is plume impingement which can lead to degradation of spacecraft surfaces through ion impact sputter erosion. This erosion can lead to possible structural, thermal, electrical, optical, or other property degradation of various components. Depending on the nature of the specific EP device, its operating conditions, and the local geometry of spacecraft surfaces relative to the thruster(s), the flux of ions can vary widely in total fluence and energy. Even in regions of high angles away from the main core of the ion beam plumes, there will be a finite amount of deflected and charge exchange ions. In many cases, the ion energies, while relatively low (< 100 eV), can still be high enough to erode non-negligible amounts of material for missions with long EP operation durations. The goal of this work is to survey the sputter yields and characteristics of a number of relevant materials as

---

[1] Aerospace technologist, Electric propulsion systems branch, john.t.yim@nasa.gov.

reported in the available literature, perform Bayesian analyses to apply fit formulas and calculate the resulting uncertainties, and to provide general guidelines for applying these sputter yields to assess spacecraft erosion. Reviews of available ion impingement sputtering measurements, modeling, and theory are a continuing process that steadily improve as we obtain more data.[2,3] This survey certainly builds upon past work and it is expected to continue to evolve as new data and methods become available.

Sputter yields have a strong dependence on the species of the incident bombarding particles. Here, we focus on xenon data only, as xenon is the primary propellant that most state-of-the-art higher power EP devices are designed, tested, and flown with. A number of other propellant options have been and are currently being pursued for EP utilization, including other noble gases, iodine, ionic liquids, other dual-mode chemical propellants, and even in-situ collected gases among several options. The sputter yields and resulting erosion characteristics will need to be specifically reevaluated for those propellant choices.

II.   Background and Approach

A. Available sputter yield measurements and uncertainties

The estimation of thruster and spacecraft component life in the presence of EP plumes is fraught with relatively high uncertainties. The typical approach is to model an in-space plume profile and then assess the resulting erosion rate from the material sputter yield based on the plume properties at the plume-surface interface. Even focusing on just the sputter yield side of the equation—ignoring the uncertainties in the projected plume properties at high angles from the thrust axis for the moment—presents a number of challenges. The available sputter yield data for various materials tend to be rather sparse, and extrapolation to the range of interest can introduce high error. Even for regions where sputter yield data are available, there can be high uncertainties and conflicting results from different laboratories. Finally, even if the measurement data can be assumed to be precise and accurate, there are uncertainties in translating the yield results from laboratory conditions to actual in-space conditions. Table 1 has an incomplete list of sources of uncertainty in the measurement and application of various sputter yields reported in literature. Note that these uncertainties can apply to either or both the laboratory measurement and/or the application of the yield data to estimate in-space erosion rates. Many of these are discussed in further detail elsewhere,[4] but some will be highlighted here below.

Table 1: Sputter yield data uncertainty sources

Category	Uncertainties
Ion energy	Ion energy distribution function width and shape Multiply-charged ions and charge exchange ions Surface potentials especially for insulators or poorly grounded/biased samples
Ion incident angle	Beam divergence Surface roughness and local incident angle
Ion flux	Current density spatial profile Secondary electron emission High ion flux vs. low flux conditions
Ion fluence	Evolution of surface roughness and amorphization of surface layers Ion implantation Total measured erosion and signal-to-noise ratio
Material	Material density in converting atomic, mass, and volume yields Crystal orientation, grain size, distribution, defects/voids Preferential erosion and species ratios (surface vs bulk) in multi-component materials Bulk material vs thin foil vs thin deposited film
Contamination	Absorption/adsorption of contaminants (e.g. water vapor, nitrogen, etc.) Oxide layer formation or other reactive surface interactions Re-deposition of sputtered target material or from other sputtered facility surfaces
Environment	Facility backpressure during sputtering process Material temperature Sample tensile/bending loads while sputtering

2

There are three primary properties of the ion source that need to be properly characterized for impingement erosion calculations: the ion energy, incident angle, and flux (current density). Sometimes the assumption is made that these properties are relatively uniform and that the ion properties are well characterized by single values across the area of interest. However, in reality, each of the three parameters are better characterized as distributions. For example, for the ion energy, results are typically interpreted as the yield from a monoenergetic beam though there will nearly always be a finite distribution width. At very low energies, the distribution tail at the upper end can significantly drive the overall yield. Similarly, double or higher multiple-charged ions can drive the overall yield. Near threshold energies, relatively small changes in ion energy can result in yields that are orders of magnitude higher. For an ion source beam with a double-to-single charged ion current ratio of $R_c = I_{++}/I_+$ and a double-to-single energy yield ratio of $R_y = Y_{++}/Y_+$, then the resulting yield ratio over an assumed single-charged ions only beam will be

$$\frac{Y \text{ (with doubles)}}{Y \text{ (only singles)}} = 1 + \frac{R_y}{2} \frac{R_c}{1 - R_c} \tag{1}$$

This is plotted in Figure 1, and it can be seen for low energies near the threshold where the gradient in the yield with energy is steep and Y_{++}/Y_+ can be very high, the effect can be significant. At higher energies, where the yield ratio is lower, the effect is diminished but still present. Conversely, a population of lower energy charge exchange ions—and high energy charge exchange neutrals—within the sputter facility can also result in a skewed interpretation of laboratory results and estimates of the total erosion rate. In addition to the ion source, the target material properties can also affect the ion beam properties at impingement. For example, a non-negligible surface potential can develop for insulating or improperly grounded materials, and the ion energies can then be further accelerated or decelerated prior to surface impact.[5,6]
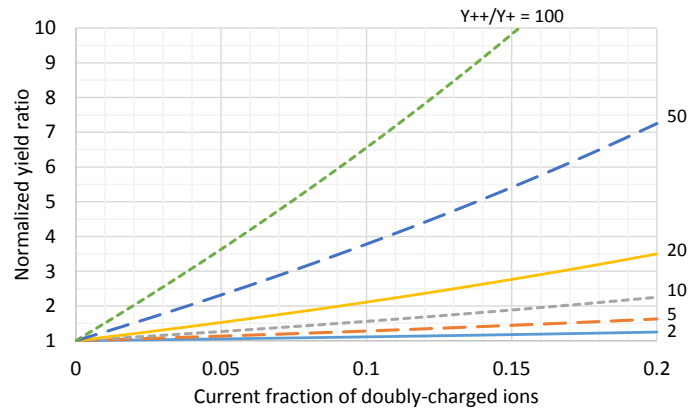

Figure 1: Change in total yield due to double-charged ions

Any angular distributions due to beam divergence or oblique electric fields should also be well characterized. Material surface roughness can also affect the local incident angle.[7,8] Furthermore, the surface roughness can change as a surface erodes under ion bombardment. Both effects of roughening[7,9] and smoothing[10,11] have been documented, as well as neither effect, where no significant change in surface roughness is observed[7,10,12,13], which makes it difficult to know in advance what level of surface roughness will occur during testing of a new material. Some multi-component materials including alloys, ceramics, glasses, and composites may have an exaggerated issue of this effect due to their non-homogeneity. The formation of microstructures from preferential component sputtering rates and differing grain or fiber erosion will affect the local sputter yield.[14-18] Even for pure elemental materials, the configuration of the crystal lattices or other highly anisotropic structures (such as the hexagonal layers of graphite) relative to the ion beam direction and surface normal has been seen to result in different sputter yields for certain conditions.[19,20] It is presumed that for most multi-component materials, eventually a steady state is reached where the immediate surface becomes enriched in the lower sputter yield elements. Depending on the expected total fluence for the duration of the space mission, the erosion could be better characterized by either the steady-state or the initial preferential sputtering.

Proper characterization of the current density profile is required to convert an erosion rate into a sputter yield or vice-versa. Uncertainties in the current collected or in the area which it is collected over will impact the reported sputter yield. Secondary electron emission (SEE) from the target material will directly affect the measured current and should be accounted for, and it can also impact the sheath and resulting surface potential for certain materials. One

3

other aspect that may also need to be considered is the effect of absolute ion flux on the sputter rate. If the ions impact the surface at a rate faster than previous ion impact energies can be locally dissipated by the material, the sputter rate may be accelerated compared to a surface which has sufficient time to locally relax after each ion impact. Too low a flux, however, can be adverse depending on the facility backpressure as discussed further below. In addition to the flux, the total ion fluence may also have uncertain effects on the sputter yield. As described above, the surface roughness may be affected over a period of ion bombardment. Certain materials may also form an amorphous layer after ion bombardment which may have a different yield than a crystalline or other structured surface.[21,22] Higher fluences will also develop a concentration of implanted ions that may affect the yield.[21,23] Generally, it is recommended sputter yield measurements employ higher fluences to remove the transient effects as the surface layer evolves with respect to roughness, amorphization, and ion implantation. In addition, the higher fluences should also result in improved measurements as the total amount of erosion will also be higher and reduces some of the relative uncertainty in the erosion measurement.

Other test and facility variables can also have an impact on the accurate measurement of sputter yields. For one, the presence of contaminant species on and near the surface layers can also affect the sputter yield. These can include absorbed or adsorbed gas or vapor molecules,[24,25] oxide layers,[26] or other contaminants. The material samples under test need to be handled and treated appropriately such that these factors are either effectively eliminated or properly characterized and accounted for. Long duration (high fluence) sputtering can help remove the presence and effect of contaminating species and surface layers, but this is also dependent on the facility capability. Poor facility pumping will not sufficiently remove contaminants. One criterion put forth on acceptable background pressures is that the yield times the ion flux should well exceed the background flux times an effective sticking coefficient, γ.[4,27]

$$Y\frac{j}{e} \gg \gamma \frac{n}{4}\sqrt{\frac{8kT}{\pi m}} \quad \rightarrow \quad P \ll \frac{Y}{\gamma}\frac{j}{e}\sqrt{2\pi mkT} \tag{2}$$

As an illustration, a background presence of water vapor at room temperature where a fraction of 0.1 is assumed to stick or react with the target material surface and is used to calculate the partial pressure flux that is less than 10 times a given ion current density multiplied by a sputter yield level. Resulting data at different conditions are shown in Figure 2. In addition, several reported sputter yield test facility base pressures and current densities are shown for comparison. Though this pressure guideline is approximate, it can still be seen that achieving conditions to measure very low sputter yields quickly becomes rather stringent. In addition to the relative particle flux at the target surface, high background pressures can also reduce the mean free path for charge exchange and other collisions affecting the behavior of the ions and sputtered particles near the target. Also of interest is the rather wide range in reported experimental conditions shown in Figure 2 with both current density and the facility base pressure spanning several decades each. Other potential impacts of these variations may not yet be fully understood. Ionization and subsequent redeposition of sputtered material, even originating from other facility surfaces impacted by the ion beam, can also affect the final results and could be affected by both variables. A few other conditions may influence sputter yields including material temperature and mechanical loads.
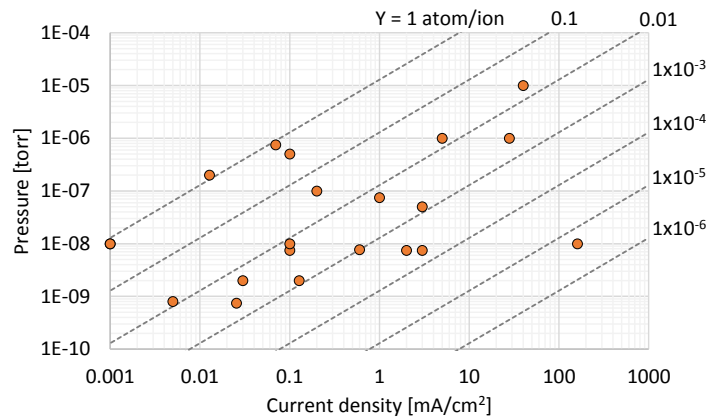

Figure 2: Reported sputter test facility base pressures and current densities along with the yield guidelines of Eq. (2) and described in the text.

4

The material sample form is another factor that should be considered for impacts to the sputtering yield. As mentioned above, even the crystalline structure of various materials can have an effect, and it would be imagined to be even more pronounced for multi-component materials where grain (or other feature) size and distribution can impact the resulting sputter yield. The material formation methods and processing (e.g. deposited films, sintered, rolled, annealed, polished, etc.) can impact the bulk or surface microstructure or the density of the resulting material, which again may affect the resulting yields.

There have been a fair number of investigations reported in literature on sputter yield assessment of various materials. Many of these result from the nuclear energy and materials processing fields where plasma interaction with materials needs to be characterized well. Unfortunately, many times, these investigations do not overlap EP characterization needs, as the ion source and species, the ion energies, or the target materials are out of scope of typical EP implementation. For most state-of-the-art EP devices, namely gridded ion engines and Hall effect thrusters, the propellant of interest is xenon gas, and for regions of the plume where impingement is likely to occur, the ion energies are relatively low, on the order of hundreds of eV or less. So available data in these ranges, for the materials of interest to spacecraft interaction, are limited. All of these considerations point to a need for a measured approach in evaluating the available data for application to spacecraft erosion from EP plumes.

B. Sputter yield energy dependence at normal incidence models

A number of empirical and semi-empirical equations to describe the sputter yield as a function of the ion energy and incidence angle have been proposed and used over the years. Most of these fits assume the energy and angular dependence of the sputter yield are independent of each other. Specifically, the energy dependence is typically calculated for yields at normal incidence and then the angular dependence is then subsequently applied as a multiplicative factor,

$$Y(E,\theta) = Y(E,0) \cdot Y'(\theta) \qquad (3)$$

There are fundamental issues with this approach that will introduce some level of error. For example, the sputter threshold energy is not necessarily constant across different incidence angles, particularly for scenarios where the projectile ion mass is significantly greater than the surface atom mass.[28,29] For the case of xenon, this will be true in most cases as xenon has a relatively high atomic mass compared to most other elements under consideration. However, there is yet no detailed theoretical development to date that adequately addresses this phenomena. Another item that affects the accuracy of these equations is that the angular portion of the sputter yield equations is typically applied as a factor to the energy dependence sputter yield at normal incidence. Since the sputter yield at normal incidence is often lower than yields at other incidence angles, the absolute errors on experimental measurements of materials at normal incidence will translate into larger relative errors which in turn are then further exacerbated at other incidence angles. However, most of the existing literature is based on the Eq.(3) assumption, perhaps primarily driven by experimental constraints and available data. This work will continue to follow this approach, but it is recommended that further advances in establishing yield curves consider a comprehensive approach with both ion energy and incident angle inherent in the derivation.

Most of the existing sputter yield curve formulas have been developed and applied to elemental materials. Certain parameters in these equations, such as the screening length, are dependent on the atomic numbers and atomic masses of the projectile ion and target atom, which are ill-defined for multi-component target materials. In addition, preferential sputtering and/or polyatomic cluster sputtering are not distinctly addressed by these models either. Hence, their application to non-elemental materials may not fully capture their sputter characteristics. A large portion of available sputter yield data has been collected for high energy ion impacts in the keV and higher range, but limited data exist in the low energy range. The difficulties associated with accurate measurement of low energy sputter yields have also resulted in poorer validation and matching of these sputter yield equations to low energy sputtering. However, keeping these caveats in mind, some of the more notable formulas that exist to describe basic energy dependent sputter yield relations are provided below in Table 2. Note that this is certainly not a comprehensive list, but just a subset of various semi-empirical sputter yield relations developed over the years.

Table 2: Energy dependence at normal incidence sputter yield formulas

Name	Original monatomic formula	Generalized form	Free parameters
Sigmund[30]	$Y = 0.042 \dfrac{\alpha}{U_s} S_n$	$Y = Q s_n$	Q
Bohdansky[31]	$Y = 0.042 \dfrac{\alpha}{U_s} \dfrac{R_p}{R} S_n \left[1 - \left(\dfrac{E_{th}}{E}\right)^{\frac{2}{3}}\right]\left[1 - \dfrac{E_{th}}{E}\right]^2$	$Y = Q s_n \left[1 - \left(\dfrac{E_{th}}{E}\right)^{\frac{2}{3}}\right]\left[1 - \dfrac{E_{th}}{E}\right]^2$	Q, E_{th}
Yamamura[32]	$Y = 0.042\, Q \dfrac{\alpha^*}{U_s} \dfrac{S_n}{1 + \Gamma k_e \epsilon^{0.3}} \left[1 - \sqrt{\dfrac{E_{th}}{E}}\right]^s$	$Y = Q s_n \left[1 - \sqrt{\dfrac{E_{th}}{E}}\right]^s$	Q, s, E_{th}
Eckstein[33,34]	$Y = Q s_n \dfrac{\left(\dfrac{E}{E_{th}} - 1\right)^\mu}{\dfrac{\lambda}{w} + \left(\dfrac{E}{E_{th}} - 1\right)^\mu}$ $w = \epsilon + 0.1728\sqrt{\epsilon} + 0.008\epsilon^{0.1504}$	$Y = Q s_n \dfrac{\left(\dfrac{E}{E_{th}} - 1\right)^\mu}{\dfrac{\lambda}{w} + \left(\dfrac{E}{E_{th}} - 1\right)^\mu}$	Q, λ, μ, E_{th}
Wilhelm[35]	$Y = \dfrac{h_{2/1}}{24} \dfrac{\sigma(E_{th})}{E_{th}^2} N^{2/3} \left(\dfrac{(M_s/M_i)^2}{1 + 2M_s/M_i}\right)^{3/2} (E - E_{th})^2$	$Y = Q \left(\dfrac{E}{E_{th}} - 1\right)^2$	Q, E_{th}

Most of the energy dependent sputter yield relations in Table 2 are based on Sigmund's original formulation,

$$Y = \frac{3}{4\pi^2} \frac{2}{\pi \lambda_0 a_{BM}^2} \frac{\alpha}{U_s} S_n \approx 0.042 \frac{\alpha}{U_s} S_n \tag{4}$$

where the dimensionless parameter $\lambda_0 = 24$ and α is another dimensionless parameter that accounts for the effect of mass ratio between the ion and surface atom and the incident angle.[30] That leaves the nuclear stopping cross section,

$$S_n = 4\pi a_L \frac{e^2}{4\pi\varepsilon_0} Z_i Z_s \frac{M_i}{M_i + M_s} s_n \tag{5}$$

as the sole term with a dependence on ion energy. In turn, it is proportional to the reduced nuclear stopping power, s_n. Several forms of s_n have been proposed and the Thomas-Fermi (TF) potential form,

$$s_n^{TF} = \frac{3.441\sqrt{\epsilon} \ln(\epsilon + 2.718)}{1 + 6.35\sqrt{\epsilon} + \epsilon\left(6.882\sqrt{\epsilon} - 1.708\right)} \tag{6}$$

has been traditionally used. However, it has been acknowledged that the Thomas-Fermi form is generally too high for application at low impact energies.[36,37] A form based on the Krypton-Carbon (KC) potential,

$$s_n^{KC} = \frac{0.5 \ln(1 + 1.2288\epsilon)}{\epsilon + 0.1728\sqrt{\epsilon} + 0.008\epsilon^{0.1504}} \tag{7}$$

is now generally preferred. Other formulated potentials, such as ZBL, could also be presumably used to calculate the nuclear stopping power at low energies. The reduced nuclear stopping power is typically expressed as a function of a reduced energy,

$$\epsilon = \frac{a_L}{Z_i Z_s} \frac{4\pi\varepsilon_0}{e^2} \frac{M_s}{M_i + M_s} E \tag{8}$$

6

where the Lindhard screening length is

$$a_L = \left(\frac{9\pi^2}{128}\right)^{1/3} a_0 \left(Z_i^{2/3} + Z_s^{2/3}\right)^{-1/2} \tag{9}$$

Since the front terms of Sigmund's equation (4) are not dependent on the ion energy, they can for simplicity be folded into an empirical scaling parameter, Q, that is dependent on the ion and target surface species as well as the incident angle, and the yield can then be expressed in a generalized form as $Y = Q s_n$.

Sigmund's formulation, however, did not take into account certain mechanisms present for low energy sputtering as it was originally derived assuming linear collision cascades are the dominant mechanism of sputtering events. Several of the assumptions in the derivation of the Sigmund form do not hold for very heavy or light ions, nor for low energies or grazing incidence angles.[30] Both Bohdansky and Yamamura introduce correctional terms to try to adapt Sigmund's derivation to include these other regimes. For example, they both introduce a factor of $1 - (E_{th}/E)^{1-m}$ to account for the decrease in the sputter yields near the threshold energy to relax certain assumptions of the primary recoil atoms, where m here is an exponent used in a generalized power law interatomic potential. Bohdansky recommends $m = 1/3$, while Yamamura uses $m = 1/2$ to cover a broader range of energies.[31,38] The particular value of m is not well defined and is dependent on energy, but for low energies m has been generally approximated to lie between zero and 1/3. Bohdansky has a second additional term based on the threshold energy, $(1 - E_{th}/E)^2$, to account for the momentum distribution of the recoiling target atoms. Both Bohdansky and Yamamura also expand their relations to cover light ion sputtering as well. These will not be considered in depth here, but the additional terms are either independent of energy (e.g. R_p/R) and can be subsumed into the scaling parameter, Q, or are largely negligible for heavy ions at low energy (i.e. $\Gamma k_e \epsilon^{0.3} \ll 1$) and can be ignored for our specific regime of interest here. There is an exponent, s, for the Yamamura form that arises from the light ion derivation and is calculated as a value of 2.8 with an assumption of $m = 1$.[39] Later empirical fitting of s is generally limited to 2.5 or 2.8 across a number of target species, but the fits are applied across a wide range of ion energies.[32] Based solely on the theoretical derivation for low energy heavy ions, s may best be approximated by unity for this particular regime.

Eckstein introduces a more empirical based correction factor for the low energy sputter data.[33,34] Here the exponent μ is not strictly tied to the power law assumed m, but becomes a free parameter for fitting. Another parameter, λ, is used to trigger the onset of the decrease. One of the reasons behind these adaptations is that the Bohdansky and Yamamura additions are relatively fixed profiles that ramp down the yield as the threshold energy is approached, but have achieved limited accuracy in describing experimentally measured profiles. To highlight this, generalized forms of the sputter formulas are shown in Table 2 and the additional low energy terms based on the threshold energy can be more clearly seen. These additional terms are plotted below in Figure 3 to further highlight their transition from zero near the threshold energy to unity at high energies. Both the Bohdansky and Yamamura forms are relatively locked into limited profile shapes independent of the species involved. Unfortunately, matching both the sputter yield profile shape and a threshold energy to available data with these equation forms has been found to be wanting. Of course the tradeoff with the Eckstein form is that there are more free parameters involved and will thus be very dependent on the data available for fitting.
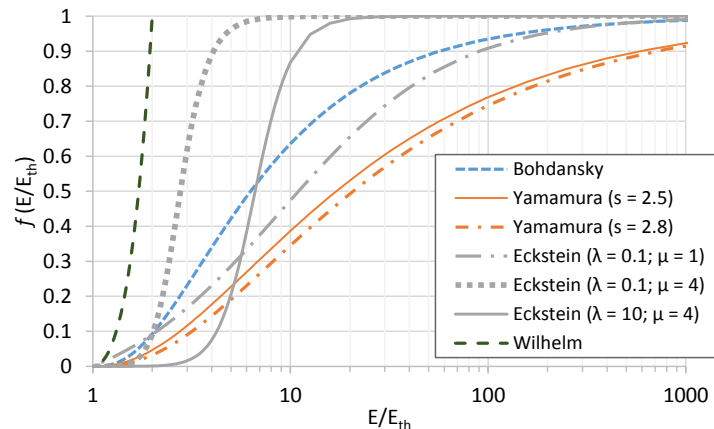

Figure 3: Sputter yield fit threshold energy transition functions

7

Finally, the last sputter yield curve presented is one by Wilhelm based on quantum-statistical analysis for very low energy sputtering near the threshold energy.[35] Here, the special low energy case of a three body sputtering mechanism is considered and a generalized relation of $Y = Q(E/E_{th} - 1)^2$ is derived. This relation is not applicable at higher energies, but shows fair agreement for around tens of volts above the threshold. While this formula is not further examined here due to the relatively narrow set of cases the analysis assumptions apply to, it is presented as an interesting alternative approach from the other ones above based on Sigmund's original work.

With any of these sputter yield formula, the free parameters, whether one or several, typically require some available data to fit them for use. For the Yamamura or Eckstein formulas, a number of fit parameters for some elemental species have been previously provided based on available data, though these fits are based on a relatively wide range of incident energies and may be of limited use for low energy yield accuracy.[32,34] Others have tried to remove some of the purely empirical or free parameter fitting aspects of the Bohdansky and Yamamura formulas by providing semi-empirical relations based on material properties.[36,40] In the absence of any measurement data to correlate a sputter yield curve, these relations can be used as first-order approximations for elemental materials, but should be taken into account with appropriate margins when applied to EP plume erosion cases.

One parameter in particular, the threshold energy value, is difficult to assess experimentally or analytically, yet strongly influences the curve fits. There have been many attempts to define it in a semi-empirical manner.[32,33,36,41] For the elemental materials, a strong dependence to the surface binding energy (often taken to be the heat of sublimation, if known) and the mass ratio has been noted. However, the threshold energy can show a notable amount of scatter from these parameters. In addition, extrapolation of these relations outside the ranges where the fits are derived can lead to serious error. For example, carbon, which has a relatively high heat of sublimation and a very low molecular mass ratio with xenon, drives the calculated threshold energy estimates from these semi-empirical relations to be rather high, well above 100 eV. However, sputter experiments with graphite have shown detectable sputter yields for xenon ion energies below 50 eV. Since an incorrect threshold energy can introduce significant error for calculated sputter yields at low ion energies, special care must be taken in the values used for curve fitting as further described in the approach below.

A special note should be taken regarding multi-component materials including alloys, oxides, ceramics, plastics, and composites among others. The formulation of the yield formulas above assumed elemental materials where the atomic number and mass are well defined. Even the unit of the resulting sputter yield, atoms per ion, is only cleanly defined for a monatomic material (hence sputter yields are sometimes provided in units of volume per ion fluence, mm^3/C for example). Specifics of multi-component material sputtering is complex involving preferential sputtering and potential effects of mesoscale structure (e.g. grains or fibers) and deserves a dedicated treatment of its own. As a first-order approximation, however, the yield formula still can be applied in a general sense. The reduced energy in Eq.(8) above can be approximated with effective atomic number and mass based on mole fraction weighted averages. The reduced nuclear stopping power, s_n^{KC}, is plotted in Figure 4 to show the relative differences across a range of elements from relatively light (e.g. carbon) to heavy (e.g. gold) from xenon ion bombardment. The differences in s_n^{KC} for the energy range of interest is limited to approximately a factor of two. Since most multi-component materials of practical interest are primarily composed of lighter elements, the differences will be even lower and using averaged values will be generally adequate. The primary influence on the yield functions near the threshold energy are from the different proposed transition functions, which do not require atomic number or mass in the calculation. Since the conversion of the atoms/ion sputter yield to a volumetric or linear erosion rate involves the molecular mass and material density, the averaged molar mass can be used again as a first-order estimate though this assumes the sputtering occurs in a stoichiometric fashion. As an alternative, the curve fitting routine can be applied directly to data in units of mm^3/C (or equivalent) to avoid the conversions. Again, this is just a simple first-order approximation; accurate characterization of multi-component material sputtering should examine the assumptions more thoroughly.
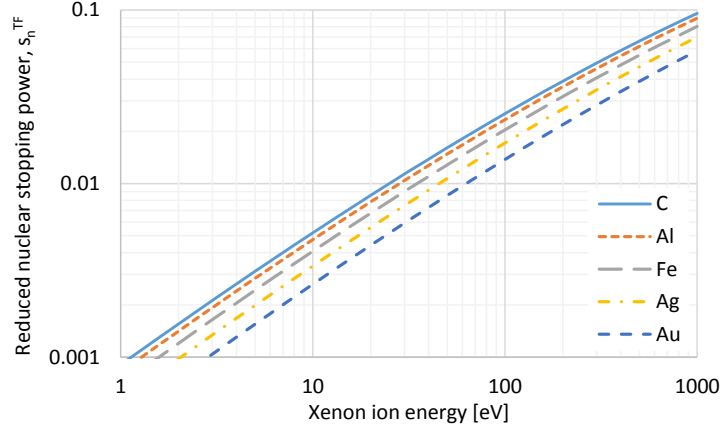
Figure 4: Reduced nuclear stopping power for xenon ion impacts with various elements.

C. Sputter yield angular dependence models

A selection of proposed angular dependence portions of the sputter yield from Eq.(3) are presented in Table 3. For Yamamura's formula, the free parameters, f and θ_{opt}, are found to be dependent on not only the species, but also the ion energy. A few semi-empirical fits of these parameters are also provided to help guide the estimates for these parameters, though again these fits have varying degrees of agreement with the available experimental data.[29,36] These semi-empirical fits are based in turn on the Sigmund f_s parameter and the average lattice constant R_0, which are tabulated by Yamamura for a number of elements.[42] Eckstein builds on the general Yamamura form, but includes additions to account for problems that arise for low incident energies and self-bombardment.[33] The three free parameters there for the angular fit are also generally dependent on the ion energy, though no semi-empirical relations are provided to guide the parameter value selection for energies with no data available for fitting and comparison.

Table 3: Angular dependence sputter yield formulas

Name	Formula	Free parameters
Yamamura[29,*]	$Y' = (\cos\theta)^{-f} \exp\left[f \cos\theta_{opt}\left(1 - (\cos\theta)^{-1}\right)\right]$ $f = f_s\left(1 + 2.5\dfrac{\sqrt{E_{th}/E}}{1 - \sqrt{E_{th}/E}}\right)$ $\theta_{opt} = \dfrac{\pi}{2} - \dfrac{286}{180}\pi\psi^{0.45}$ $\psi = \left(\dfrac{a_L}{R_0}\right)^{3/2}\sqrt{Z_1 Z_2 \left(Z_1^{2/3} + Z_2^{2/3}\right)^{-1/2}\dfrac{1}{E}}$	f, θ_{opt}
Eckstein[33,†]	$Y' = (\cos\theta^c)^{-f}\exp\left[b\left(1 - (\cos\theta^c)^{-1}\right)\right]$	f, b, c
Wei[43]	$Y' = \dfrac{\alpha}{A}\cos\theta\exp\left(\dfrac{a^2}{2\alpha^2}\left[1 - \dfrac{\alpha^2}{A^2}\cos^2\theta\right]\right)$ $A^2 = \alpha^2\cos^2\theta + \beta^2\sin^2\theta$	a, α, β

*The Yamamura equation and variables shown here were formulated for heavy ions
†The Eckstein formula shown here assumes noble gas ions

Wei extends Sigmund's original theoretical formulation to examine angular effects.[43] Here, the parameters correlate to the projected energy range, a, and the longitudinal and transverse straggling ranges, α and β, respectively. The equation can be reformulated as

$$Y' = \frac{1}{\sqrt{1 + (\beta/\alpha)^2 \tan^2\theta}}\exp\left(\frac{1}{2}\left(\frac{a}{\alpha}\right)^2\left[1 - \frac{1}{1 + (\beta/\alpha)^2\tan^2\theta}\right]\right) \tag{10}$$

9

In this form, the formula is reduced to two effective parameters, a ratio of the transverse to longitudinal straggling ranges (β/α) and a ratio of the projected energy range to the longitudinal straggling range (a/α). These ratios can be calculated as a function of the mass ratio and a power approximation exponent, m, while being independent of ion energy.[44] For low energy conditions, $m = 1/3$ is generally a fair approximation. For xenon ions, which are relatively heavy to most target species, the ratio of the projected energy range to the longitudinal straggling range will generally be greater than one while the ratio of the transverse to longitudinal straggling range will be less than one.[44,8] Some of the reported values of the projected energy and straggling ranges used to match to experimentally measured sputter yields[43] do not appear to strictly hold to the expected theoretical values, however. For the Wei formula, the maximum yield multiplier and the angle at which it occurs are found to be

$$\theta_{max} = \tan^{-1}\sqrt{\frac{(a/\alpha)^2 - 1}{(\beta/\alpha)^2}}; \quad Y'_{max} = \frac{1}{(a/\alpha)}\exp\left(\frac{1}{2}\left(\left(\frac{a}{\alpha}\right)^2 - 1\right)\right) \tag{11}$$

D. Bayesian parameter fitting approach

The process used here to fit parameters to the available low energy xenon ion impact sputter yield data follows a Bayesian approach as also used by Eckstein.[33,45] The high levels of uncertainty in the available published data lends itself to be examined using probabilistic Bayesian data analysis. The relative disagreements in some of the published sputter yield data are much too disparate to be aleatory in nature, but rather likely indicate epistemic issues. The published literature sources of sputter yield data are not always fully descriptive of the process, variables, and potential uncertainty sources, and even the ones that are more extensive in detail do not show exhaustive accounting of all potential variables. The effects of even one uncontrolled or unconsidered variable (e.g. multiply-charged ions, charge exchange ions, secondary electron emission, oxide layers or other contaminants, improper grounding, etc.) could potentially be substantial. Due to these unknowns, the realized uncertainty on the published yields may be significantly greater than the stated error bars typically ranging from 50% to just a few percent. Even comparing sets of data from two different laboratories, the published yields can vary by over an order of magnitude in some cases. For the purposes of EP plume spacecraft interaction, where ion current densities can range by orders of magnitude with relatively small changes in position, and where mission throughput requirements can also vary significantly, an estimate of the overall magnitude of the sputter yields may be sufficient for most general purposes. In addition, since the total erosion is calculated by multiplying the yield with the current density and the total duration or throughput, it is really the multiplicative, rather than the additive, uncertainties that are of interest. For the latter, a Gaussian distribution of the data and its uncertainties is often applied (unless a more relevant distribution can be specified), but for the former case that applies here, a lognormal distribution is used to describe and fit the data. Other distributions—or their logarithmic forms—may also be considered such as the Jeffreys or the Cauchy distributions as they have a longer tail than the normal and may be more accommodating of outlier data points. A generous 3σ uncertainty of a factor of two is assigned for the results presented here, in part due to the nature of the available data as described above, but also to broaden the resulting phase space for examination of yield fit trends.

The Bayesian approach is used here to generate posterior probability distributions of the coefficients for a given sputter yield model as described in the sections above applied to a given data set for a particular material. To accomplish this, the available data set for each material—split into the energy dependence at normal incidence and the angular dependence at set energies—is processed through a nested sampling routine based on a Markov chain Monte Carlo (MCMC) approach.[45] This procedure can be applied to any of the fit models described above. As discussed above with reference to Figure 3, and shown via examples later, the Eckstein model is the primary energy dependent fit used here as the others are sometimes insufficient to describe the measured low energy trends. For the angular yield dependence, the Wei fit formula will generally be applied.

To generate the posterior probability distribution functions, the prior probability distributions and the likelihood functions need to be supplied. Since not much is known about the parameters ahead of time, apart from general bounds, uniform priors are assigned. The bounds for each parameter is guided by past results of parameter estimation. As will be discussed later, the threshold energy parameter has an outsized influence on the very low energy region. Here a lower bound of 5 eV is imposed as spectroscopic measurements have detected sputtering events for as low as 10 eV xenon ion impacts.[10,46,47] The likelihood function is based on the lognormal distribution as mentioned above and calculates the relative multiplicative error for each data point from the assumed sample yield function. The MCMC method begins with a randomized set of the fit formula parameters across the prior distributions for each. Then with the nested sampling algorithm, the parameter set with the worst likelihood function is randomly re-assigned to a set with a higher likelihood. This procedure is iterated to map the posterior pdf in n-dimensional space with increasing

likelihood where n is the number of parameters for a given sputter yield fit formula. The process eventually converges on the parameter set with maximum likelihood. These best fit values are certainly useful in estimating sputter yields, but perhaps of equal importance are the corresponding posterior pdfs which allow for uncertainty estimation that can be used to set an appropriate margin philosophy. These MCMC models are typically run with 4500 objects (parameter sets) and 100,000 iterations, though these are adjusted as needed for proper phase space coverage and convergence depending on the data set being examined.

III. Results and Discussion

A step through of the data analysis and curve fitting process for molybdenum is shown here first as an example as there is a relative wealth of available sputter yield data from low energy xenon bombardment. Sample posterior pdfs from applying the MCMC approach to the Eckstein energy dependent sputter yield formula as shown for each pair of its four fitting parameters in Figure 5. The sample posterior pdfs are colored to highlight the likelihood contours with the maximum likelihood values presented as the dots at the center of the contours. A few observations can be made from this representation, including the relative correlation and covariance between pairs of parameters. For example, the clearest relation appears to be between λ and E_{th} where a negative correlation is observed. The parameter μ also appears to exhibit trends with respect to each of the three other parameters, while Q does not show particularly strong relations with either λ or E_{th}. The threshold energy parameter is mostly limited at the upper end around 15 eV, primarily due to the lowest energy experimental data point at that value. The values of the parameters that provide the maximum likelihood and the ranges that bracket the 50% likelihood (a rough equivalent of FWHM, and shown by the black contour in Figure 5) are shown in Table 4. It should be noted that these ranges should not be taken independently of each other, as shown by the correlated pdfs in Figure 5. A similar process was followed for the Bohdansky and Yamamura formulas, as was done with the Eckstein, and the best fits for each of the formulas to the molybdenum data are shown in Figure 6. Here it can be seen that the trend of the measured data does not easily fit into the Bohdansky or Yamamura curve forms at the low energy range. The Eckstein form, with its additional parameters, is able to fit the data more successfully.
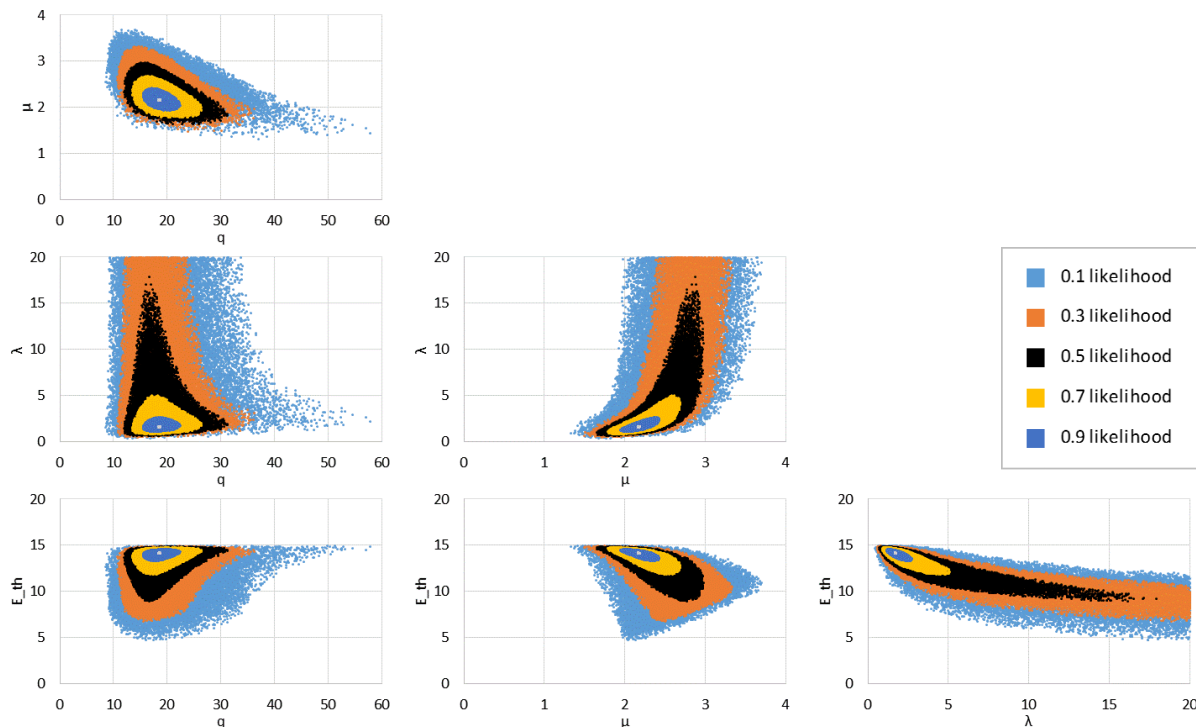

Figure 5: Posterior samples at various likelihood levels for each pair of parameters for the Eckstein formula for xenon-molybdenum sputtering

Table 4: MCMC maximum likelihood values of the Eckstein formula parameter bracketed by the 50% likelihood ranges for xenon-molybdenum sputtering

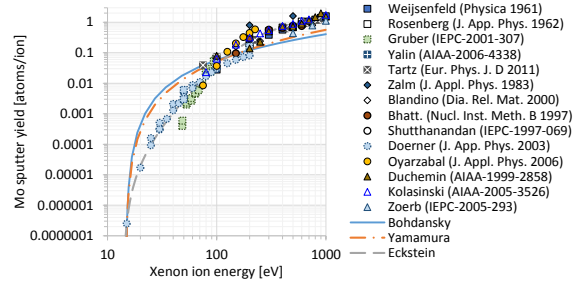| Parameter	Value
Q	18.4 $^{-6.1}/_{+11.7}$
μ	2.2 $^{-0.5}/_{+0.8}$
λ	1.7 $^{-0.8}/_{+14.6}$
E_{th}	14.2 $^{-4.9}/_{+0.7}$

Figure 6: Molybdenum sputter yields from low energy xenon ions at normal incidence and compared to different sputter yield formulas

In contrast with molybdenum, most materials have a relative dearth of available data or data with notable disagreement with each other, and the optimal parameter ranges and their relations will not be so clear cut. As an example, there are relatively sparse data available regarding sputter yields of aluminum from low energy xenon ion impacts. The same MCMC procedure is applied and the maximum likelihood Eckstein curve (blue line) as well as yield ranges bracketing the 50% likelihood curves (gray shaded area) are shown on the top-left side of Figure 7. Since no experimental measurements are available below 100 eV, the uncertainty in the low energy curve is significant and many potential solutions may be applicable.

Another highlighted case is for gold where differences in measured yield from different references are significant below 100 eV as seen on the top-right side of Figure 7. In the absence of an applied discriminator—this may include throwing out suspect data points—the data analysis approach outlined above will only effectively split the difference of disparate data sets to generate yield curves that lie between the data. However, in many cases, it is difficult to clearly mark down one set of results over another as both likely are subject to a number of uncertainties as touched upon earlier in this report. In contrast, two more material data sets are also shown in Figure 7, where more measurements are available and agreement is better. Consequently, the yield ranges bracketing the 50% likelihood curves are also correspondingly tighter together.
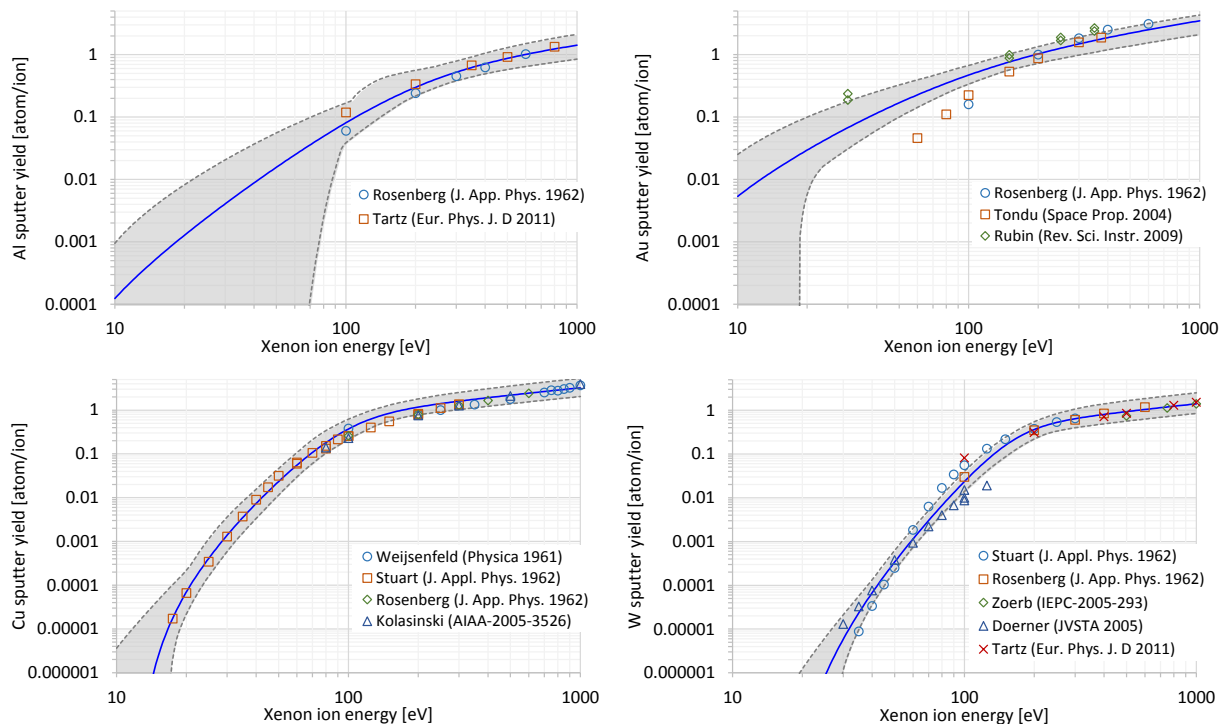

Figure 7: Aluminum (top-left), gold (top-right), copper (bottom-left), and tungsten (bottom-right) sputter yields from low energy xenon ions at normal incidence with measured data compared to 50% likelihood bounds on the yield curves.

12

A conservative approach for erosion calculations may be to use the upper 50% likelihood limit in yield as a bracket. The data is then generally aligned with measurements where measured values are available, but provides some margin and likely very conservative estimates of the sputtering at very low energies. Table 5 lists parameter sets for the Eckstein curves for both the best fit results and these conservative 50% likelihood upper bounds. Values which are at the imposed bounds are marked with an asterisk. In some instances, the best fit results already require a threshold energy near the imposed bound of 1 eV, and no further lower threshold energy is then available. Additional conservatism can be imposed over the entire curve by adding margin to the scaling factor Q. This latter adjustment could be applied to either the conservative upper estimate or to the maximum likelihood best fit.

Table 5: MCMC results of the maximum likelihood values and a conservative upper range for fitting the Eckstein energy dependent sputter yield formula to low energy xenon ion impacts on elemental materials at normal incidence

Material	Max. likelihood (best fit)				50% likelihood upper range				Data refs.
	Q	λ	μ	E_{th}	Q	λ	μ	E_{th}	
C(gr)	4	0.8	1.8	21	6	28	2.2	6	8,10,18,20,48-51
Al	17	1.5	1.5	5	23	0.3	1.3	5	11,48
Si	11	5.0	1.7	5	18	0.2	1.1	5	22,48
Ti	6	56	3.0	7	10	80	3.1	6	10,11,48,52
Cr	57	0.2	1.3	11	82	0.8	1.5	5	47,48,53
Mn	32	0.08	1.3	33	43	0.7	1.3	6	48
Fe	22	0.2	1.6	20	35	0.6	1.4	6	26,48,54
Co	29	12	1.9	5	67	17	1.8	5	47,48
Ni	26	5.9	1.8	5	40	1.5	1.5	5	48,54,55
Cu	41	2.4	3.1	12	63	55	3.5	6	46,48,54,56
Mo	19	1.8	2.2	14	28	12	2.6	8	10,11,22,48,49,54-64
Ag	65	0.05	1.8	26	78	4.6	2.4	5	11,48,65
Ta	19	0.2	2.6	38	31	55	3.6	14	10,25,34,48
W	23	32	4.0	16	41	56	3.7	13	10,11,24,46,48,62
Au	61	0.06	1.0	5	74	0.02	1.0	5	48,65,66

Apart from the fits to elemental materials in Table 5, the analysis approach was also applied to multi-component materials with available data. The reduced energy parameter is estimated by mole-weighted averages where known or by the approximate predominant constituent. Again, the total impact to the yield curve can be largely subsumed into the scaling factor Q. Results are shown below in Table 6 including the ratios of ϵ/E that are used. Since the units of sputtered atoms per ion as previously used for the elemental materials is not clearly defined for multi-component materials, the scaling factor Q is fit here to the more directly applicable units of mm^3/C. Two exceptions are for the two metallic alloys Invar and Kovar, which are left in units of atoms/ion, as that is how the experimental data are reported.

Table 6: MCMC results of the maximum likelihood values and a conservative upper range for fitting the Eckstein energy dependent sputter yield formula to low energy xenon ion impacts on non-elemental materials at normal incidence

Material	ϵ/E	Max. likelihood (best fit)				50% likelihood upper range				Data refs.
		Q	λ	μ	E_{th}	Q	λ	μ	E_{th}	
Invar	1.4×10^{-6}	75	0.2	1.9	36	79	94	3.5	9	49
Kovar	1.4×10^{-6}	19	0.3	1.2	5	28	0.05	0.9	5	12
SiO$_2$	1.8×10^{-6}	1.4	0.01	1.0	59	2.4	0.04	1.0	11	5,6,57,67
Coverglass	1.8×10^{-6}	0.8	0.1	1.0	5	1.4	0.03	0.8	6	15,64,68
MgF$_2$	1.9×10^{-6}	0.8	0.08	2.1	80	1.3	260	2.9	8	64,68
ITO	1.2×10^{-6}	9	0.1	2.0	80	14	0.1	0.8	5	69,70
Al$_2$O$_3$	1.9×10^{-6}	0.3	2.8	1.6	5	0.5	0.3	1.1	5	6,67
Kapton	2.0×10^{-6}	0.9	49	2.2	7	1.8	7.3	1.8	5	5,9,57
C-C composite	2.0×10^{-6}	3.5	0.8	1.3	5	5	0.05	1.0	5	13,18,50,61

It should be noted that while the reduced energy may be approximated by an average of the constituents, the yield curve parameters or the yield value itself will typically not be well approximated by an average of the yield of the constituents. The sputter yield is a strong function of the surface binding energy, which in turn is dependent on bond strengths and other parameters that can differ significantly from the monatomic arrangements. For example, the limited metallic alloy sputter data available in Invar (an iron and nickel alloy) and Kovar (an iron, nickel, and cobalt alloy) do

13

not show significant adherence to the yields of their constituents. Likely similar effects will be seen for other alloys, though some common aerospace alloys such as 6061 aluminum alloy or grade 5 titanium alloy have near 90% or greater composition of the primary metal and perhaps they may be satisfactorily approximated by their main constituent. Direct data and comparisons will be required to confirm, however.

The angular dependent yield curves from Wei, et al. were also analyzed against available data and are presented in Table 7. The maximum yield multiplier and angle are also calculated via Eq. (11) and are also tabulated. Again, due to the sparse data sets and relatively high uncertainties in the results, some caution should be applied in using these provided curves, where only the maximum likelihood values are provided below. Additional margin can applied as needed.

Table 7: MCMC results of the maximum likelihood values for fitting the Wei angular dependent sputter yield formula to low energy xenon ion impact data

Material	Max. likelihood (best fit)				Data refs.
	β/α	a/α	θ_{max}	Y'_{max}	
Al	0.97	2.05	62°	2.4	11,71
Ti	1.18	2.41	62°	4.6	11,52
Mo	1.07	1.90	56°	1.9	11,52,56,57,62
Ag	1.35	1.81	48°	1.7	11,65
Ta	1.17	1.55	45°	1.3	62
W	1.02	1.57	50°	1.3	11,62
Au	1.67	1.92	44°	2.0	66
C(gr)	0.88	2.20	66°	3.1	8,13,18,50,52
C-C composite	0.66	2.21	71°	3.2	13,18,50,61
SiO$_2$	0.97	1.92	59°	2.0	5,57,67,72
Coverglass	1.15	2.70	65°	8.6	15,64,68
Al$_2$O$_3$	0.71	2.48	73°	5.3	67
MgF$_2$	1.08	2.87	68°	13	64,68
ITO	1.09	2.14	60°	2.8	69
Kapton	1.02	1.90	58°	1.9	5,9,57

Conclusions

The determination of accurate sputtering yields to apply in erosion calculations is fraught with uncertainties. A survey of existing yield measurement data and sputter yield formulas was undertaken and assessed for the best approach in analyzing the available data and distilling it into appropriate curves for EP plume impingement erosion calculations. A Bayesian approach, through use of a nested sampling Markov chain Monte Carlo routine, is taken here to process the available data and provide best fits as well as conservative extensions, particularly when regarding the very low energy region near the threshold energy. Since the results are particularly dependent on the data available, these values should continue to evolve as additional sputter yield measurements are made. A deep dive into the measurement approaches and stated uncertainties for each available data source may be able to provide a more tailored fit as well, but often not all the necessary information is published. Thus, a healthy margin is recommended for application to spacecraft integration.

Acknowledgments

References

[1]Herman, D. A., et al., "Overview of the development and mission application of the advanced electric propulsion system (AEPS)," *35th International Electric Propulsion Conference*, IEPC-2017-284, 2017.

[2]Boyd, I. D., and Falk, M. L., "A review of spacecraft material sputtering by Hall thruster plumes," *37th AIAA/ASME/SAE/ASEE Joint Propulsion Conference & Exhibit*, AIAA-2001-3353, 2001.

[3]Duchemin, O. B., et al., "A review of low energy sputtering theory and experiments," *25th International Electric Propulsion Conference*, IEPC-97-068, 1997.

[4]Andersen, H. H., and Bay, H. L., "Sputtering yield measurements," *Sputtering by particle bombardment I*, Topics in Applied Physics, v. 47, ed. Behrisch, R., Springer-Verlag, 1981.

[5]Yalin, A. P., Rubin, B., Domingue, S. R., Glueckert, Z., and Williams, J. D., "Differential sputter yields of boron nitride, quartz, and kapton due to low energy Xe+ bombardment," *43rd AIAA/ASME/SAE/ASEE Joint Propulsion Conference & Exhibit*, AIAA-2007-5314, 2007.

[6]Tartz, M., Heyn, T., Bundesmann, C., and Neumann, H., "Measuring sputter yields of ceramic materials," *31st International Electric Propulsion Conference*, IEPC-2009-240, 2009.

[7]Küstner, M., Eckstein, W., Dose, V., and Roth, J., "The influence of surface roughness on the angular dependence of the sputter yield," *Nuclear Instruments and Methods in Physics Research B*, v. 145, pp. 320-331, 1998.

[8]Kolasinski, R. D., Polk, J. E., Goebel, D., and Johnson, L. K., "Carbon sputtering yield measurements at grazing incidence," *42nd AIAA/ASME/SAE/ASEE Joint Propulsion Conference & Exhibit*, AIAA-2006-4337, 2006.

[9]Tondu, T., Viel-Inguimbert, V., and Darnon, F., "Erosion of materials used on satellite external skin by electric propulsion," *28th International Electric Propulsion Conference*, IEPC-2003-257, 2003.

[10]Doerner, R. P., Whyte, D. G., and Goebel, D. M., "Sputtering yield measurements during low energy xenon plasma bombardment," *Journal of Applied Physics*, v. 93, n. 9, pp. 5816-5823, 2003.

[11]Tartz, M., Heyn, T., Bundesmann, C., Zimmermann, C., and Neumann, H., "Sputter yields of Mo, Ti, W, Al, Ag under xenon ion incidence," *The European Physical Journal D*, v. 61, pp. 587-592, 2011.

[12]Eichhorn, C., et al., "Sputter yield measurements of thin foils using scanning transmission ion microscopy," *The European Physical Journal D*, 69: 19, 2015.

[13]Williams, J. D., Johnson, M. L., and Williams, D. D., "Differential sputtering behavior of pyrolytic graphite and carbon-carbon composite under xenon bombardment," *40th AIAA/ASME/SAE/ASEE Joint Propulsion Conference & Exhibit*, AIAA-2004-3788, 2004.

[14]Smentkowski, V. S., "Trends in sputtering," *Progress in Surface Science*, v. 64, pp. 1-58, 2000.

[15]Garnier, Y., Viel, V., Roussel, J.-F., and Bernard, J., "Low-energy xenon ion sputtering of ceramics investigated for stationary plasma thrusters," *Journal of Vacuum Science and Technology A*, v. 17, n. 4, pp. 3246-3254, 1999.

[16]Schinder, A. M., Walker, M., and Rimoli, J. J., "Three-dimensional model for erosion of a Hall-effect thruster discharge channel wall," *Journal of Propulsion and Power*, v. 30, n. 5, pp. 1373-1382, 2014.

[17]Duan, X., et al., "Ion sputtering erosion mechanisms of h-BN composite ceramics with textured microstructures," *Journal of Alloys and Compounds*, v. 613, pp. 1-7, 2014.

[18]Deltschew, R., et al., "Sputter characteristics of carbon-carbon compound material," *27th International Electric Propulsion Conference*, IEPC-01-118, 2001.

[19]Zhou, X. W., Wadley, H. N. G., and Sainathan, S., "Low energy sputtering of nickel by normally incident xenon ions," *Nuclear Instruments and Methods in Physics Research B*, v. 234, pp. 441-457, 2005.

[20]Hechtl, E., and Bohdansky, J., "Sputtering behavior of graphite and molybdenum at low bombarding energies," *Journal of Nuclear Materials*, v. 122 & 123, pp. 1431-1436, 1984.

[21]Blank, P. and Wittmaack, K., "Energy and fluence dependence of the sputtering yield of silicon bombarded with argon and xenon," *Journal of Applied Physics*, v. 50, pp. 1519-1528, 1979.

[22]Zalm, P. C., "Energy dependence of the sputtering yield of silicon bombarded with neon, argon, krypton, and xenon ions," *Journal of Applied Physics*, v. 54, pp. 2660-2666, 1983.

[23]Sinha, M. K., "Sputtering of metals with low-energy inert gas ions: possible influence of trapped gas," *Journal of Applied Physics*, v. 39, pp. 2150-2152, 1968.

[24]Winters, H. F., and Sigmund, P., "Sputtering of chemisorbed gas (nitrogen on tungsten) by low-energy ions," *Journal of Applied Physics*, v. 45, pp. 4760-4766, 1974.

[25]Mantenieks, M. A., Foster, J. E., Ray, P. K., Shutthanandan, S. V., and Thevuthasan, T. S., "Low Energy Xenon Ion Sputtering Yield Measurements," *27th International Electric Propulsion Conference*, IEPC-01-309, 2001.

[26]Williams, J. D. and Corey, R. L., "Influence of residual gases on witness plate measurements during Hall-effect thruster testing," *Plasma Sources Science and Technology*, v. 19, 025020, 2010.

[27]Yonts, O. C., and Harrison Jr., D. E., "Surface cleaning by cathode sputtering," *Journal of Applied Physics*, v. 31, pp. 1583-1584, 1960.

[28]Eckstein, W., Garciá-Rosales, C., Roth, J., and László, J., "Threshold energy for sputtering and its dependence on angle of incidence," *Nuclear Instruments and Methods in Physics Research Section B: Beam Interactions with Materials and Atoms*, v. 83, n. 1-2, pp. 95-109, 1993.

[29]Yamamura, Y., "An empirical formula for angular dependence of sputtering yields," *Radiation Effects*, v. 80, pp. 57-72, 1984.

15

[30]Sigmund, P., "Sputtering by ion bombardment: theoretical concepts," *Sputtering by particle bombardment I*, Topics in Applied Physics, v. 47, ed. Behrisch, R., Springer-Verlag, 1981.

[31]Bohdansky, J., "A universal relation for the sputtering yield of monatomic solids at normal ion incidence," *Nuclear Instruments and Methods in Physics Research Section B*, v. 2, i. 1-3, pp. 587-591, 1984.

[32]Yamamura, Y., and Tawara, H., "Energy dependence of ion-induced sputtering yields from monatomic solids at normal incidence," *Atomic Data and Nuclear Data Tables*, v. 62, pp. 149-253, 1996.

[33]Eckstein, W., and Preuss, R., "New fit formulae for the sputtering yield," *Journal of Nuclear Materials*, v. 320, pp. 209-213, 2003.

[34]Eckstein, W., "Sputtering yields," *Sputtering by particle bombardment*, Topics in Applied Physics, v. 110, eds. Behrisch, R. and Eckstein, W., Springer, 2007.

[35]Wilhelm, H. E., "Quantum-statistical analysis of low energy sputtering," *Australian Journal of Physics*, v. 38, pp. 125-133, 1985.

[36]Garciá-Rosales, C., Eckstein, W., and Roth, J., "Revised formulae for sputtering data," *Journal of Nuclear Materials*, v. 218, pp. 8-17, 1994.

[37]Wilson, W. D., Haggmark, L. G., and Biersack, J. P., "Calculations of nuclear stopping, ranges, and straggling in the low-energy region," *Physical Review B*, v. 15, n. 5, pp. 2458-2468, 1977.

[38]Yamamura, Y., "Contribution of anisotropic velocity distribution of recoil atoms to sputtering yields and angular distributions of sputtered atoms," *Radiation Effects*, v. 55, pp. 49-56, 1981.

[39]Yamamura, Y., Matsunami, N., and Itoh, N., "Theoretical studies on an empirical formula for sputtering yield at normal incidence," *Radiation Effects*, v. 71, pp. 65-86, 1983.

[40]Seah, M. P., "An accurate semi-empirical equation for sputtering yields, II: for neon, argon and xenon ions," *Nuclear Instruments and Methods in Physics Research B*, v. 229, pp. 348-358, 2005.

[41]Bohdansky, J., "An analytical formula and important parameters for low-energy ion sputtering," *Journal of Applied Physics*, v. 51, i. 5, pp. 2861-2865, 1980, and v. 52, i. 3, p. 1610, 1981.

[42]Yamamura, Y., Itikawa, Y., and Itoh, N., "Angular dependence of sputtering yields of monatomic solids," *IPPJ-AM-26,* 1983.

[43]Wei, Q., Li, K.-D., Lian, J., and Wang, L., "Angular dependence of sputtering yield of amorphous and polycrystalline materials," *Journal of Physics D: Applied Physics*, v. 41, 172002, 2008.

[44]Winterbon, K. B., Sigmund, P., and Sanders, J. B., "Spatial distribution of energy deposited by atomic particles in elastic collisions," *Matematisk-Fysiske Meddelelser*, Kongelige Danske Videnskabernes Selskab, v. 37, n. 14, 1970.

[45]Sivia, D. S., and Skilling, J., *Data Analysis: A Bayesian Tutorial*, 2nd edition, Oxford University Press, 2006.

[46]Stuart, R. V., and Wehner, G. K., "Sputtering yields at very low bombarding energies," *Journal of Applied Physics*, v. 33, 2345, 1962.

[47]Handoo, A. K., and Ray, P. K., "Sputtering of cobalt and chromium by argon and xenon ions near the threshold energy region," *Canadian Journal of Physics*, v. 71, 155, 1993.

[48]Rosenberg, D. and Wehner, G. K., "Sputtering yields for low energy He+-, Kr+-, and Xe+- ion bombardment," *Journal of Applied Physics*, v. 33, n. 5, pp. 1842-1845, 1962.

[49]Gruber J. R., "Low-energy sputter erosion of various materials in a T5 ion thruster," *27th International Electric Propulsion Conference*, IEPC-2001-307, 2001.

[50]Tartz, M., Neumann, H., Leiter, H., and Esch, J., "Pyrolytic graphite and carbon-carbon sputter behaviour under xenon ion incidence," *29th International Electric Propulsion Conference*, IEPC-2005-143, 2005.

[51]Oyarzabal, E., Doerner, R. P., Shimada, M., and Tynan, G. R., "Carbon atom and cluster sputtering under low-energy noble gas plasma bombardment," *Journal of Applied Physics*, v. 104, 043305, 2008.

[52]Williams, J. D., Gardner, M. M., Johnson, M. L., and Wilbur, P. J., "Xenon sputter yield measurements for ion thruster materials," *28th International Electric Propulsion Conference*, IEPC-2003-130, 2003.

[53]Handoo, A., K., and Ray, P. K., "Sputtering yield of chromium by argon and xenon ions with energies from 50 to 500 eV," *Applied Physics A*, v. 54, pp. 92-94, 1992.

[54]Weijsenfeld, C. H., Hoogendoorn, A., and Koedam, M., "Sputtering of polycrystalline metals by inert gas ions of low energy (100-1000 eV)," *Physica*, v. 27, pp. 763-764, 1961.

[55]Matsunami, N., et al., "Energy dependence of the ion-induced sputtering yields of monatomic solids," *Atomic Data and Nuclear Data Tables*, v. 31, pp. 1-80, 1984.

[56]Kolasinski, R., D., "Oblique angle sputtering yield measurements for ion thruster grid materials," *41st AIAA/ASME/SAE/ASEE Joint Propulsion Conference & Exhibit*, AIAA-2005-3526, 2005.

[57]Yalin, A. P., Surla, V., Farnell, C., Butweiller, M., and Williams, J. D., "Sputtering studies of multi-component materials by weight loss and cavity ring-down spectroscopy," *42nd AIAA/ASME/SAE/ASEE Joint Propulsion Conference & Exhibit*, AIAA-2006-4338, 2006.

[58]Bhattacharjee, S., et al., "Application of secondary neutral mass spectrometry in low-energy sputtering yield measurements," *Nuclear Instruments and Methods in Physics Research B*, v. 129, pp. 123-129, 1997.

[59]Shutthanandan, V., et al., "On the measurement of low-energy sputtering yield using Rutherford backscattering spectrometry," *25th International Electric Propulsion Conference*, IEPC-97-069, 1997.

[60]Duchemin, O. B., and Polk, J. E., "Low energy sputtering experiments for ion engine lifetime assessment: preliminary results," *35th AIAA/ASME/SAE/ASEE Joint Propulsion Conference & Exhibit*, AIAA-1999-2858, 1999.

[61]Blandino, J. J., Goodwin, D. G., and Garner, C. E., "Low energy sputter yields for diamond, carbon-carbon composite, and molybdenum subject to xenon ion bombardment," *Diamond and Related Materials*, v. 9, pp. 1992-2001, 2000.

[62]Zoerb, K. A., Williams, J. D., Williams, D. D., and Yalin, A. P., "Differential sputtering yields of refractory metals by xenon, krypton, and argon ion bombardment at normal and oblique incidences," *29th International Electric Propulsion Conference*, IEPC-2005-293, 2005.

[63]Oyarzabal, E., Yu, J. H., Doerner, R. P., Tynan, G. R., and Schmid, K., "Molybdenum angular sputtering distribution under low energy xenon ion bombardment," *Journal of Applied Physics*, v. 100, 063301, 2006.

[64]Noushkam, N., et al., "Sputtering effects of xenon ion thruster plume on common spacecraft materials," *AIAA SPACE 2015 Conference and Exposition*, AIAA-2015-4642, 2015.

[65]Tondu, T., Inguimbert, V., Darnon, F., and Roussel, J. F., "Angular characterisation of erosion and contamination by electric propulsion," *4th International Spacecraft Propulsion Conference*, ESA SP-555, 2004.

[66]Rubin, B., Topper, J. L., Farnell, C. C., and Yalin, A. P., "Quartz crystal microbalance-based system for high-sensitivity differential sputter yield measurements," *Review of Scientific Instruments*, v. 80, 103506, 2009.

[67]Tondu, T., Chardon, J.-P., and Zurbach, S., "Sputtering yield of potential ceramics for Hall effect thruster discharge channel," *32nd International Electric Propulsion Conference*, IEPC-2011-106, 2011.

[68]Yalin, A. P., Topper, J. L., Farnell, C. C., Yoder, G., Hoang, B., and Corey, R., "Effect of ion sputtering on transmission of coverglass with magnesium fluoride coating," *32nd International Electric Propulsion Conference*, IEPC-2011-066, 2011.

[69]Kannenberg, K., Khayms, V., Emgushov, B., Werthman, L., and Pollard, J. E., "Validation of Hall thruster plume sputter model," *37th AIAA/ASME/SAE/ASEE Joint Propulsion Conference & Exhibit*, AIAA-2001-3986, 2001.

[70]Fife, J. M., Gibbons, M. R., VanGilder, D. B., and Kirtley, D. E., "Initial use of a 3-D plasma simulation system for predicting surface sputtering and contamination by Hall thrusters," *33rd Plasmadynamics and Lasers Conference*, AIAA-2002-2125, 2002.

[71]Provost, S., Theroude, C., and Chèoux-Damas, P., "Overview of Astrium erosion / contamination modelling tool and validation on ONERA experimental results," *9th International Symposium on Materials in a Space Environment*, ESA SP-540, 2003.

[72]Rizzo, A., Alvisi, M., Sarto, F., Scaglione, S., and Vasanelli, L., "The influence of ion mass and energy on the composition of IBAD oxide films," *Surface and Coatings Technology*, v. 108-109, pp. 297-302, 1998.